AGU PUBLICATIONS

JGR

Journal of Geophysical Research: Space Physics

BRIEF REPORT

10.1002/2013JA019481

Key Points:
- First successful forecast of SSW with the online-coupled IDEA model
- First successful forecast of ionospheric response to SSW with the IDEA model
- Predicted ionospheric change corresponds well to SW2 amplitude and phase change

Correspondence to:
H. Wang,
Houjun.Wang@noaa.gov

Citation:
Wang, H., R. A. Akmaev, T.-W. Fang, T. J. Fuller-Rowell, F. Wu, N. Maruyama, and M. D. Iredell (2014), First forecast of a sudden stratospheric warming with a coupled whole-atmosphere/ionosphere model IDEA, *J. Geophys. Res. Space Physics*, *119*, 2079-2089, doi:10.1002/2013JA019481.

Received 1 OCT 2013
Accepted 3 MAR 2014
Accepted article online 10 MAR 2014
Published online 28 MAR 2014

First forecast of a sudden stratospheric warming with a coupled whole-atmosphere/ionosphere model IDEA

H. Wang[1,2], R. A. Akmaev[2], T.-W. Fang[1,2], T. J. Fuller-Rowell[1,2], F. Wu[1,2], N. Maruyama[1,2], and M. D. Iredell[3]

[1]CIRES, University of Colorado Boulder, Boulder, Colorado, USA, [2]Space Weather Prediction Center, NOAA, Boulder, Colorado, USA, [3]NOAA, Environmental Modeling Center, College Park, Maryland, USA

Abstract We present the first "weather forecast" with a coupled whole-atmosphere/ionosphere model of Integrated Dynamics in Earth's Atmosphere (IDEA) for the January 2009 Sudden Stratospheric Warming (SSW). IDEA consists of the Whole Atmosphere Model and Global Ionosphere-Plasmasphere model. A 30 day forecast is performed using the IDEA model initialized at 0000 UT on 13 January 2009, 10 days prior to the peak of the SSW. IDEA successfully predicts both the time and amplitude of the peak warming in the polar cap. This is about 2 days earlier than the National Centers for Environmental Prediction operational Global Forecast System terrestrial weather model forecast. The forecast of the semidiurnal, westward propagating, zonal wave number 2 (SW2) tide in zonal wind also shows an increase in the amplitude and a phase shift to earlier hours in the equatorial dynamo region during and after the peak warming, before recovering to their prior values about 15 days later. The SW2 amplitude and phase changes are shown to be *likely* due to the stratospheric ozone *and/or* circulation changes. The daytime upward plasma drift and total electron content in the equatorial American sector show a clear shift to earlier hours and enhancement during and after the peak warming, before returning to their prior conditions. These ionospheric responses compare well with other observational studies. Therefore, the predicted ionospheric response to the January 2009 SSW can be largely explained in simple terms of the amplitude and phase changes of the SW2 zonal wind in the equatorial *E* region.

1. Introduction

During the January 2009 sudden stratospheric warming (SSW), *Chau et al.* [2010] showed that the vertical plasma drift at the magnetic equator over Jicamarca, Peru, changed dramatically, with stronger upward drifts after dawn, reversing to downward drifts in the afternoon. The observations of total electron content (TEC) from ground-based GPS receivers were also shown to change in response to the vertical plasma drift, with a stronger equatorial ionospheric anomaly (EIA) in the morning when the drifts were stronger upward and a decrease in TEC when the drifts turned downward [*Goncharenko et al.*, 2010a]. It was suggested that the change in dayside *E* region dynamo winds in response to the stratospheric warming was responsible for the change in vertical plasma drift and TEC. More discussion of the effects of SSW on ionosphere can be found in *Chau et al.* [2011].

Fuller-Rowell et al. [2011] presented results of ionospheric response to the January 2009 SSW with an ionospheric model, the CTIPe (Coupled Thermosphere-Ionosphere-Plasmasphere electrodynamics) model [e.g., *Millward et al.*, 2001], driven offline by the hourly winds from analysis of the Whole atmosphere Data Assimilation System (WDAS) [*Wang et al.*, 2011]. Their simulation results showed good agreement with the ionospheric observations. *Jin et al.* [2012] reported simulation results of the January 2009 SSW from the Ground-to-topside model of Atmosphere and Ionosphere for Aeronomy nudged by the atmospheric analysis data. In particular, *Jin et al.* [2012] discussed how the amplitude of the semidiurnal tide increases when the north-south asymmetry of the zonal wind was reduced in the middle atmosphere during the SSW.

In this paper, we present a first *forecast* with an *online-coupled* whole-atmosphere/ionosphere model of Integrated Dynamics in Earth's Atmosphere (IDEA) to study the atmospheric tidal and ionospheric response during the January 2009 SSW. In particular, we found that changes in both amplitude and phase of the semidiurnal, westward propagating, zonal wave number 2 (SW2) tide in zonal wind in the forecast drive a clear ionospheric response that corresponds well to the observed features.

The IDEA model, including its components and coupling, is briefly described in section 2, followed by section 3 on results and discussion of a forecast for the January 2009 SSW with the coupled IDEA model, and ending with conclusions in section 4.

2. The IDEA Model

The Integrated Dynamics in Earth's Atmosphere (IDEA) model consists of the online-coupled Whole Atmosphere Model (WAM) and Global Ionosphere-Plasmasphere (GIP) model.

WAM is an extension of the National Centers for Environmental Prediction's (NCEP) Global Forecast System (GFS), extended from 64 model levels (with model top at about 60 km) to 150 model levels (with model top at about 600 km) [*Akmaev et al.*, 2008; *Akmaev*, 2011]. It covers the regions of important ionospheric processes and their variability. WAM includes basic ionospheric effects on the neutral atmosphere, i.e., ion drag and Joule heating.

GIP is derived from the Coupled Thermosphere-Ionosphere-Plasmasphere (CTIP) model [*Millward et al.*, 2001]. Its geomagnetic field is defined in the modified apex coordinates using the International Geomagnetic Reference Field. Its dynamo solver is adapted from the National Center for Atmospheric Research's Thermosphere-Ionosphere-Electrodynamics General Circulation Model [*Richmond et al.*, 1992]. The ionospheric dynamo equation in the apex coordinate was described in detail in *Richmond* [1995a]. The GIP model has been used to study the ionospheric longitudinal variability [*Fang et al.*, 2009, 2013; *Pedatella et al.*, 2011] and ionospheric responses to SSW [*Pedatella et al.*, 2012].

WAM is a Message Passing Interface (MPI) code and GIP is a serial code. The coupling between WAM and GIP involves data collection and redistribution from inside the MPI code of WAM. GIP is called inside WAM as a subroutine, concurrently exchanging necessary fields (neutral winds, temperature and neutral composition from WAM, and ion velocity, collisional frequency, and Joule heating from GIP) between WAM and GIP in the overlapping layer (about 90–600 km) at each GIP time step. The time step for WAM is 3 min, and the time step for GIP is 15 min.

To study the direct effects on ionospheric plasma drift and TEC of the predicted tidal wind changes during the January 2009 SSW, in the following we present only forecast results from the *one-way, online-coupled* IDEA model, in which WAM winds are feeding into GIP, but GIP fields are not feeding back to WAM.

3. The IDEA Model Forecast of the January 2009 SSW

The coupled whole-atmosphere/ionosphere IDEA model was used for a forecast during the January 2009 SSW. The IDEA model was initialized with the analysis from WDAS [*Wang et al.*, 2011] at 0000 UT 13 January 2013, 10 days before the peak warming. By *analysis* here we mean the best estimate of the true state of a physical system from available observations and a physically based numerical model. A 30 day forecast was performed.

In the following, we analyze the results in terms of the stratospheric forecast, as represented by the polar cap temperature changes, amplitude and phase changes of the SW2 tide, and predicted vertical plasma drift and TEC changes in the equatorial American sector. We also present a simple physical explanation of how a change in phase and amplitude of SW2 in zonal wind can drive a change in ionospheric plasma drift and TEC in terms of conventional ionospheric electrodynamics.

3.1. Forecast of the Stratospheric Temperature Change

Figure 1 shows the time series of the stratospheric polar cap temperature at 10 hPa (~30 km), averaged poleward of 60°N, from the 30 day IDEA model forecast, and compares it with the WDAS analysis. The IDEA model predicts the time and amplitude of peak warming very well, with the polar cap temperature closely following the WDAS analysis.

Shown in Figure 1 is also the average polar cap temperature at 10 hPa from the 16 day NCEP operational GFS forecast, initialized at the same time from its Global Data Assimilation System. The overall temperature change follows the analysis closely in the first 7 days. But it fails to predict a sharp peak warming occurred on 23 January 2009. Initialized 2 days later, the operational GFS model was able to predict the time and amplitude of the peak warming close to the analysis. Since there was no "tuning" for the purpose of the prediction of this specific SSW case in either of the models, the fact that IDEA can provide a better forecast in

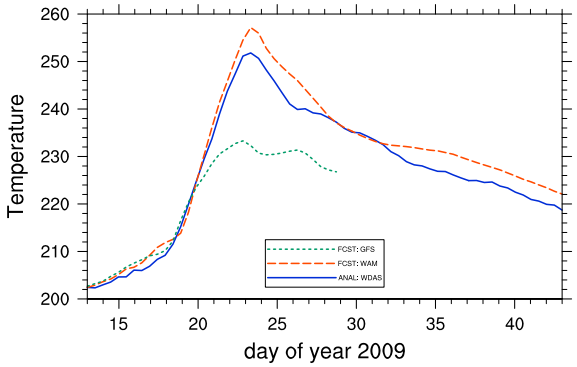

Figure 1. Time series of the mean 60°N polar cap temperature (K) at 10 hPa (~30 km): 30 day WAM forecast (long-dashed line), WDAS analysis (solid line), and 16 day operational GFS forecast (short-dashed line).

terms of the polar cap temperature in the stratosphere is likely simply due to the extended vertical dimension of IDEA. The GFS model top is at ~60 km; WAM removes this artificial lid by extending its model top to ~600 km, which is particularly important for *stratospheric* forecasts.

3.2. Forecast of the Tidal Response to SSW

The standard space-time spectral analysis technique [e.g., *Wheeler and Kiladis*, 1999] was applied to the hourly model output for the tidal wave analysis. One day data were used for each spectral analysis period. We examine the changes of both amplitude and phase of the SW2 and terdiurnal, westward propagating, zonal wave number 3 (TW3) tides. The numerical simulation study by *Millward et al.* [2001] showed that daytime vertical plasma drift is highly dependent on the magnitude and phase of the semidiurnal tide. Large variations in SW2 and TW3 amplitudes during the January 2009 SSW were found in previous studies [e.g., *Fuller-Rowell et al.*, 2011; *Wang et al.*, 2011].

Figure 2 shows the time evolution of both the amplitude and phase of the SW2 and TW3 tides in the zonal wind at about 115 km, the *key dynamo layer* in the equatorial *E* region where the daytime conductivity has a peak magnitude [e.g., *Richmond*, 1995b]. The amplitude of SW2 increased by about 20 to 40 m s^{-1} between 23 January and 10 February (Figure 2a). The phase of SW2 shifted earlier by more than 2 h during the period, before it recovered later again to the values prior to the warming (Figure 2b).

For the TW3 tide, its amplitude in the equatorial region did not increase until February; with a 10 to 20 m s^{-1} increase between 2 and 10 February, reaching about half of the SW2 amplitude around that time (Figure 2c). The TW3 tide also had similar phase changes as the SW2 tide, but more pronounced south of the equator (Figure 2d).

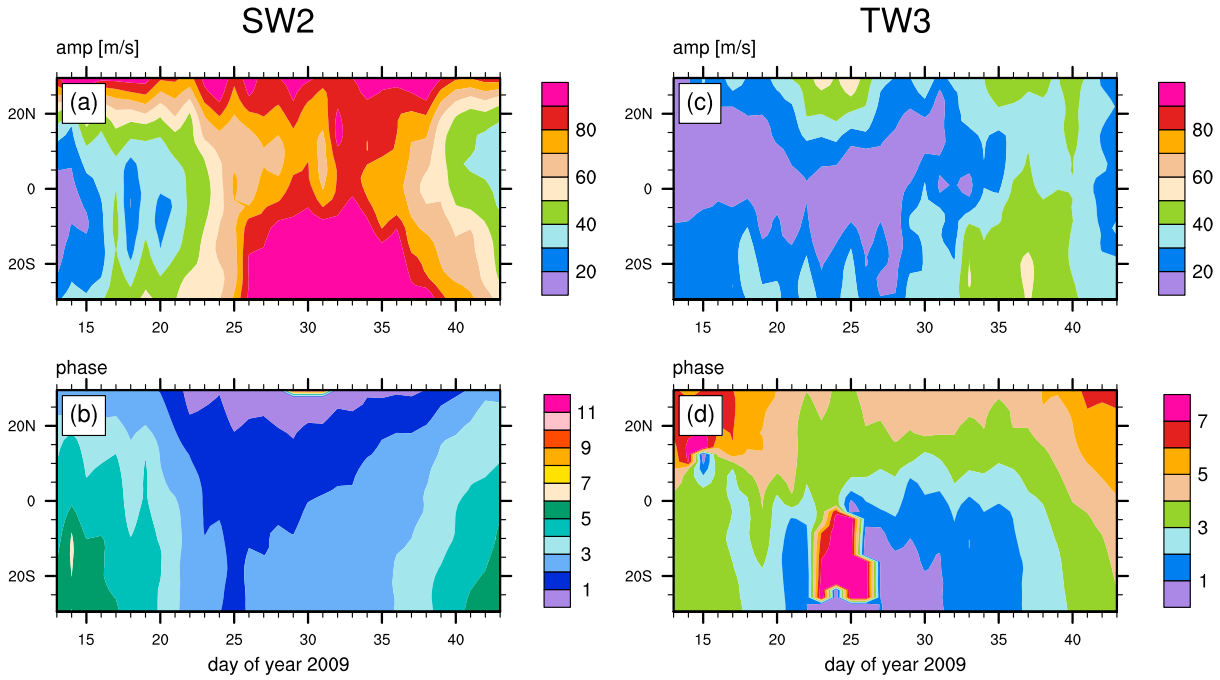

Figure 2. Time evolution of SW2 and TW3 tides in zonal wind at model level 112 (~115 km): (a) amplitude (m s^{-1}) and (b) phase (local time (LT) hour of the (first) maximum) for SW2, (c) amplitude, and (d) phase for TW3.

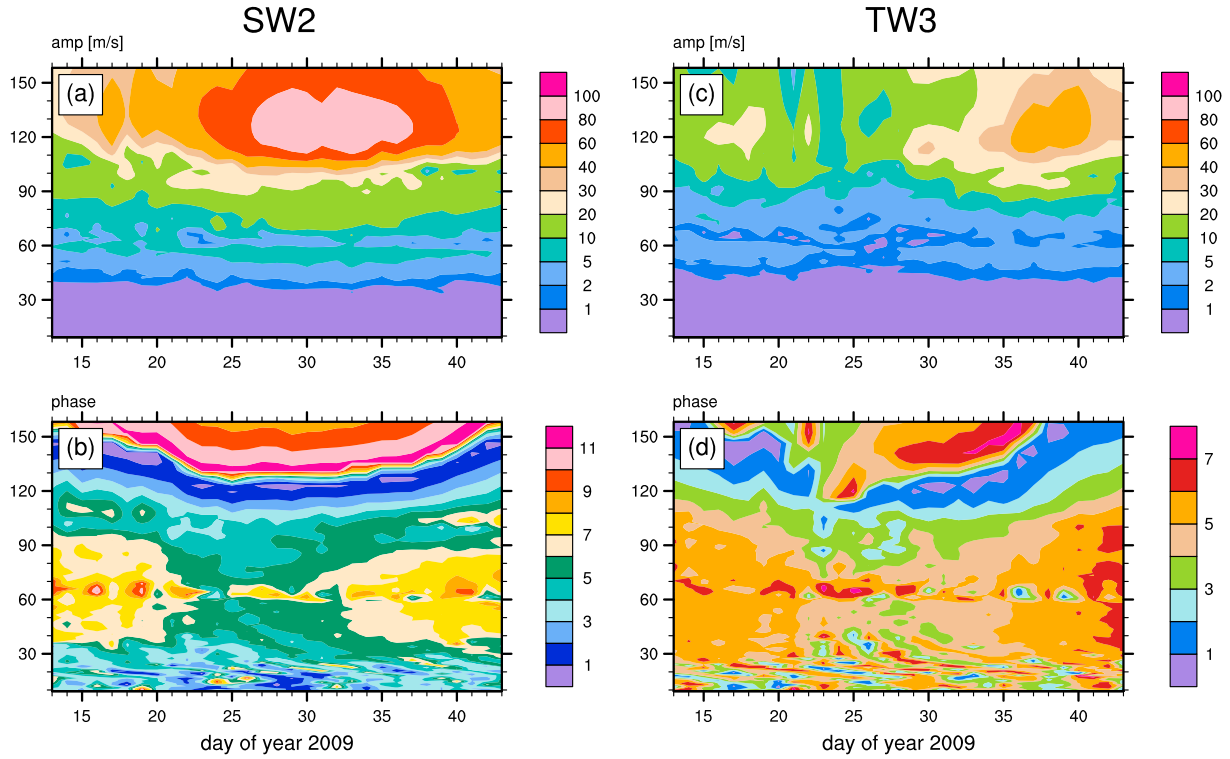

Figure 3. Time evolution of SW2 and TW3 tides in zonal wind between altitudes 10 and 160 km, averaged between latitudes 10°S and the equator: (a) amplitude (m s^{-1}) and (b) phase (local time (LT) hour of the (first) maximum) for SW2, (c) amplitude and (d) phase for TW3.

To understand the amplitude and phase changes of the SW2 and TW3 tides during the SSW, we examine their time evolution from the stratosphere to the lower thermosphere (altitudes 10 to 160 km). Figure 3 shows the time evolution of amplitude and phase, averaged between 10°S and the equator. In these low latitudes, the *E* region SW2 amplitude increased by 20–40 m s^{-1} between 23 January and 10 February, while the TW3 amplitude increased about 10 days later by about half of the magnitude, as shown in Figure 2. The phase changes for the SW2 tide started from the stratosphere (its source region).

Figure 4 is the same as Figure 3, except averaged over the middle latitudes from 40 to 50°N. In these middle latitudes, the SW2 amplitude decreased between the 100 and 130 km altitudes during the SSW peak warming period, while the TW3 amplitude increased above 110 km altitudes with two large increases (>20 m s^{-1}) between 21 and 28 January and between 2 and 10 February. This is consistent with the analysis of *Wang et al.* [2011]. The later large increase in the TW3 amplitudes also corresponds to a decrease in the SW2 tide above 140 km altitudes. This indicates that nonlinear wave-wave interactions may occur when the tide amplitudes become large, as discussed in *Wang et al.* [2011].

In the middle latitudes, the phase changes for both SW2 and TW3 started from the stratosphere, the main source regions of these tides.

To understand *why* the predicted SW2 and TW3 tides have such amplitude and phase changes during the January 2009 SSW, we examine the stratospheric ozone and related circulation changes during the period. The potential role of stratospheric ozone during the January 2009 SSW was analyzed by *Goncharenko et al.* [2012]. From our Figure 5, we can see that the mixing ratio of ozone in the tropics increased in the upper stratosphere at 2 hPa (Figure 5a) and 3 hPa (Figure 5b), and decreased in the lower stratosphere at 30 hPa (Figure 5c) during the warming period. We also found upward vertical motion in the upper stratospheric equatorial region, with an enhanced upward motion during the warming period (Figure 5d, showing $\omega = \frac{dp}{dt}$ with $\omega < 0$ for upward motion). This upward motion not only transports ozone upward from the ozone-rich lower stratosphere (Figures 5a–5c) but also induces the tropical cooling (Figure 5e), thus helps to increase the ozone lifetime in the photochemically controlled upper stratosphere [e.g., *Goncharenko et al.*, 2012].

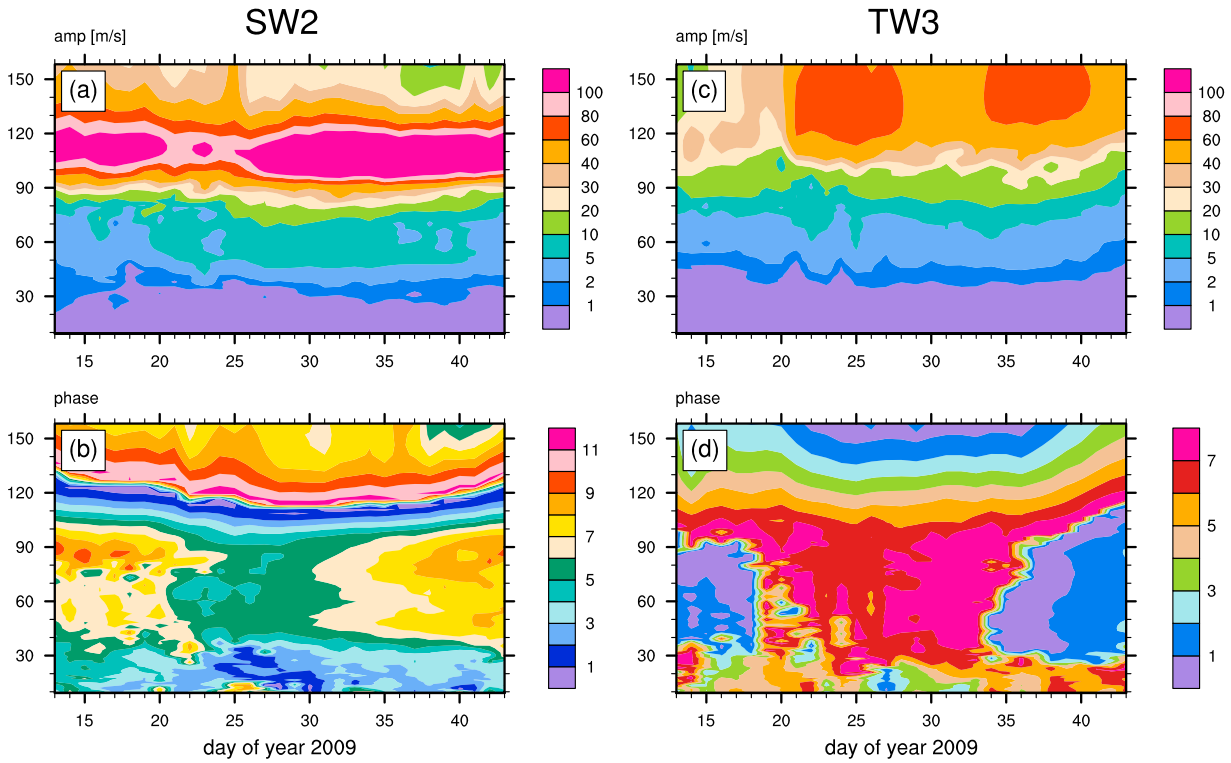

Figure 4. Same as Figure 3 except averaged between latitudes 40 and 50°N.

These changes in ozone may enhance the SW2 amplitude, according to *Goncharenko et al.* [2012]. A further detailed study of this mechanism would be beneficial.

During the SSW the zonal mean zonal winds in the stratosphere also reversed from a prevailing westerly (eastward) direction before SSW to an easterly (westward) direction (Figure 5f). This change in the wind direction reduces the north-south asymmetry of the background zonal winds and also helps to increase the SW2 amplitude, as analyzed in *Jin et al.* [2012].

This change of the wind direction is also expected to cause phase changes in the SW2 (and TW3) tides. Figures 4b and 4d show that the phase changes in the middle latitudes started from below in the source region (about 40 km). This can be understood as follows. When the prevailing winds in the stratosphere undergo a sudden directional changes from eastward to westward, the waves launched in the source region are "pushed" more in the direction of the new prevailing winds, i.e., westward. Thus, the phases of the SW2 (and TW3) tides were shifted westward or to earlier hours.

The *time-dependent* numerical simulation of the SW2 tide by *Aso* [1993] appears to support the idea that the background zonal winds can cause *transient* phase changes in the SW2 tide. In the simulation by *Aso* [1993], the equinoctial background conditions were used, with the zonal mean zonal wind having a westerly (eastward) jet of about 53 m s^{-1} at about 55 km altitude around 50°N latitude, as in *Aso et al.* [1987]. In the first 5 days of model integration (after a 2 day onset), the SW2 phase shifted eastward or to later hours for about 2 to 3 h [*Aso*, 1993, Figure 7 (top right panel)], before it reached a "steady" state. This numerical simulation result indicates that the background *eastward* wind could have caused the *eastward* phase shift in the first 5 days of the time-dependent model integration.

Therefore, the amplitude changes of the SW2 tide during the SSW can be due to the enhanced ozone in the upper stratosphere and the reduced north-south asymmetry in the stratospheric zonal mean zonal winds; the phase changes of the SW2 and TW3 tides can be mainly due to the changes (reversal) of the prevailing stratospheric zonal mean zonal winds during the SSW.

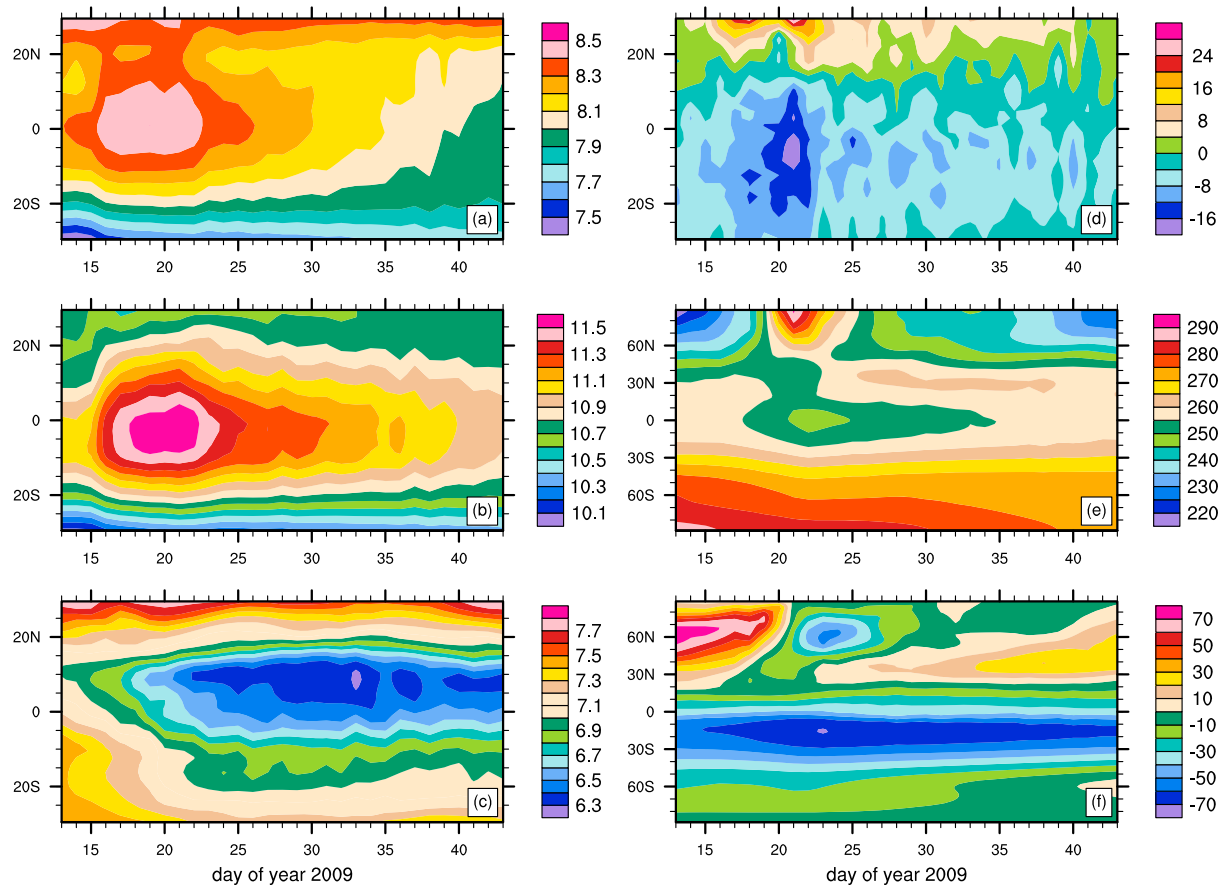

Figure 5. Time evolution of the zonally averaged fields in the stratosphere: (a) ozone mixing ratio (10^{-6} kg/kg) at 2 hPa (~43 km), (b) ozone mixing ratio (10^{-6} kg/kg) at 3 hPa (~40 km), (c) ozone mixing ratio (10^{-6} kg/kg) at 30 hPa (~25 km), (d) $\omega = \frac{dp}{dt}$ (10^{-5} Pa s^{-1}) at 2 hPa, with $\omega < 0$ for the upward vertical motion, (e) temperature (K) at 2 hPa, and (f) zonal wind [ms^{-1}] at 2 hPa.

3.3. Forecast of the Ionospheric Response to SSW

Plasma drift and TEC forecasts also show significant changes in response to SSW.

Figure 6 shows the predicted daytime vertical E×B drifts at 300 km altitude at Jicamarca (11.6°S, 76.5°W) on 15, 25, and 27 January (Figure 6a) and every third day from 30 January to 8 February (Figure 6b), together with the climatological mean calculated from the empirical model of *Scherliess and Fejer* [1999]. On 15 January, before the peak warming, the daytime vertical drift closely followed the climatological mean, with a maximum upward drift just after 1000 LT (local time). On 25 January, 2 days after the peak warming and at maximum phase shift of SW2 (Figure 2b), the vertical plasma drift had a large increase to a maximum of about 55 m s^{-1}, and its phase also shifted at least 1 h earlier to just before 0900 LT. There was also a strong downward drift in the afternoon around 1500 LT. On 27 January, the daytime vertical plasma drift exhibited a similar *semidiurnal* signature with strong upward drift in the morning and large downward drift in the afternoon, except that its phase shifted back closer to the climatological mean.

Strong semidiurnal upward and downward drifts are still seen on 30 January. A very strong upward drift around 0900 LT on 2 February corresponds to the strongest SW2 amplitudes across the equatorial region (Figure 2a). The downward drifts in the afternoon also became smaller after 2 February and disappeared on 8 February. This may be due to the decrease of the SW2 amplitude and its phase recovery, as well as the increase of the TW3 amplitude during this later period after the SSW.

Therefore, the vertical plasma drift predicted by IDEA showed a clear response to the phase and amplitude change of the SW2 tide in the zonal wind.

Figure 7 shows the predicted TEC in the low-latitude American sector on 15 January, 8 days before the peak warming, and on 27 January, 4 days after the peak warming as in *Goncharenko et al.* [2010a]. In response to

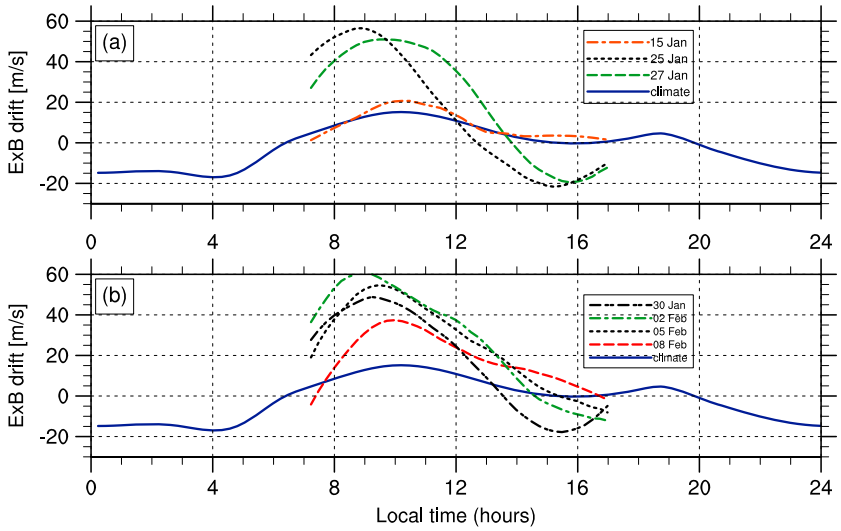

Figure 6. The daytime vertical ExB plasma drift at Jicamarca, as computed from the IDEA model forecast: (a) on 15 January (long-short-dashed line), 25 January (short-dashed line), and 27 January (long-dashed line); climatological mean is also shown (solid line); (b) every third day from 30 January to 8 February.

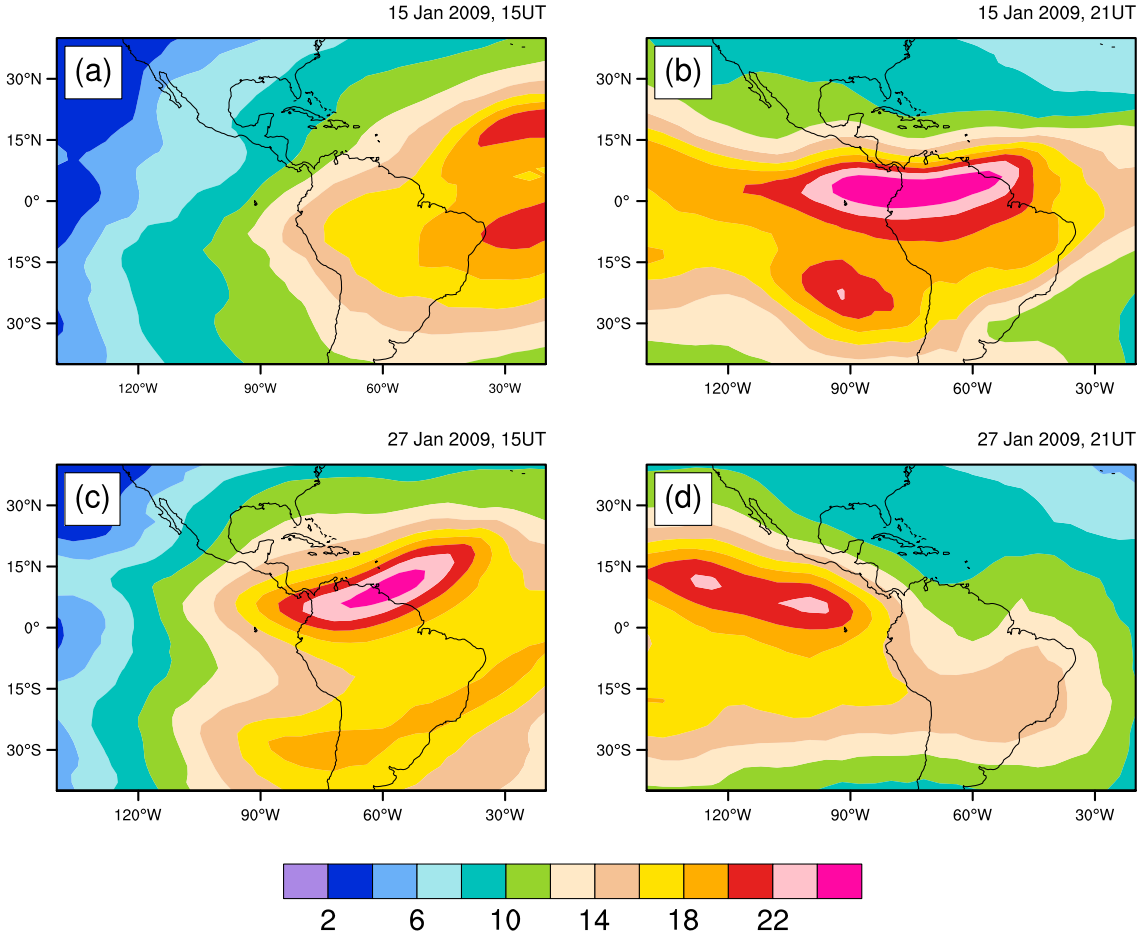

Figure 7. The TEC map in TECU (TEC unit, 10^{16} electrons/m^2) on the American sector from the IDEA model forecast: before the peak warming at (a) 1500 UT and (b) 2100 UT on 15 January 2009; after the peak warming at (c) 1500 UT and (d) 2100 UT on 27 January 2009. 1500 UT is 1000 LT (local time) and 2100 UT is 1600 LT at Jicamarca.

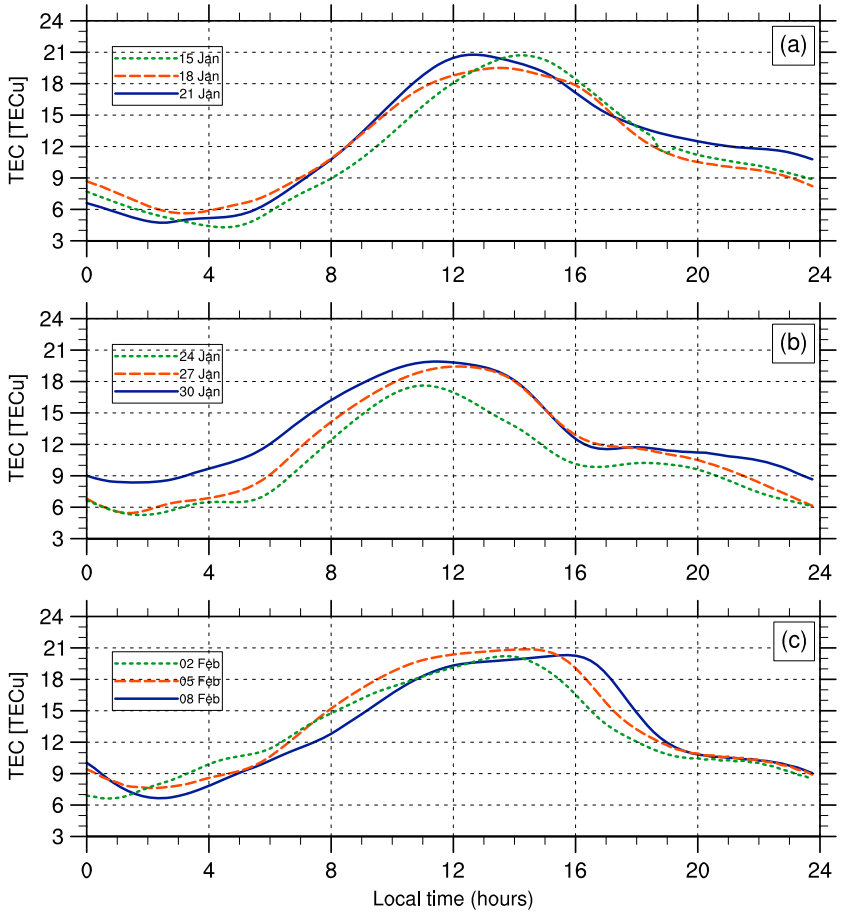

Figure 8. The local time variation of TEC in TECU, averaged from 40°S to 20°N and within ±7.5° longitudes of 75°W, every third day from 15 January to 8 February: (a) 15, 18, and 21 January; (b) 24, 27, and 30 January; and (c) 2, 5, and 8 February.

the change in the vertical plasma drift shown in Figure 6a, the TEC in the morning at 1500 UT (1000 LT at Jicamarca) exhibited a much stronger equatorial ionization anomaly (EIA), as well as a clear shift to earlier hours, i.e., a westward shift of EIA from Figures 7a–7c. In the afternoon at 2100 UT (1600 LT at Jicamarca), the EIA after the peak warming (Figure 7d) was strongly suppressed due to the strong downward drift. A westward shift of EIA can also be seen from before the peak warming (Figure 7b) to (4 days) after the peak warming (Figure 7d).

Figure 8 shows the local time variation of TEC, averaged from 40°S to 20°N and within ±7.5° longitude of 75°W, every third day from 15 January to 8 February. The peak TEC averaged over this large area showed significant local time variations: starting from its "normal" peak time at 1500 LT on 15 January (Figure 8a), shifting westward to earlier hours, peaked around 1100 LT on 24 and 30 January (Figure 8b), then shifting back eastward to later hours toward its "normal" peak time at 1500 LT on 5 February and even 1600 LT on 8 February. Similar TEC local time variations ("phase shift") were reported in *Goncharenko et al.* [2010b] and *Liu et al.* [2011].

These predicted ionospheric changes in the vertical plasma drift and TEC in response to SSW followed closely the observations, such as shown in *Goncharenko et al.* [2010a, Figure 1], *Chau et al.* [2010], *Goncharenko et al.* [2010b], and *Liu et al.* [2011].

3.4. How Can a Phase Shift in Tidal Wind Drive a Phase Shift in Plasma Drift?

The dynamo solver used to compute the (polarization) electric field follows the procedure described in *Richmond* [1995a]. In the Appendix, we discuss briefly the conventional ionospheric dynamo theory in a simplified configuration. It is shown that the *westward* zonal wind plays an important role in generating

the eastward electric field, and hence the upward vertical plasma drift; the meridional wind plays only a secondary role (equation (A4)).

As shown in Figure 2b, the maximum phase shift occurred on 25 January in the forecast, 2 days after the peak warming. For migrating tides, the phase hour is also the local time hour of the first maximum amplitude. The maximum *eastward* SW2 zonal wind occurred at 0100 LT on 25 January. Thus, the maximum *westward* SW2 zonal wind occurred 6 h later at 0700 LT. This phase shift in the SW2 wind, in combination with the diurnal variation of conductivity, drives a phase shift in the vertical plasma drift (Figure 6); the amplitude increase in the vertical plasma drift is mainly due to the increase of SW2 wind amplitude in the low latitudes. The effect of amplitude and phase of the semidiurnal tide on daytime plasma drift was also investigated in other numerical simulation study [*Millward et al.*, 2001, Figure 5].

Therefore, the predicted ionospheric response to the January 2009 SSW can be largely explained in simple terms of the phase and amplitude changes of the *E* region SW2 tide in zonal wind.

4. Conclusions

In this study, we present the first "weather forecast" for the January 2009 SSW case with the online-coupled whole-atmosphere/ionosphere model IDEA. The IDEA model produced a successful forecast of the time and amplitude of the January 2009 stratospheric warming 10 days in advance. This is about 2 days earlier than the operational GFS forecast. In addition, the coupled IDEA model also predicted an increase in amplitude and phase shift to earlier hours of the SW2 zonal wind in the equatorial dynamo region during and after the peak warming, before recovering to their prior values about 15 days later. The SW2 amplitude and phase changes are shown to be *likely* due to the stratospheric ozone *and/or* circulation changes. Shown are also the corresponding changes in the daytime plasma drift and TEC that compare well with observations. Therefore, the predicted ionospheric response to the January 2009 SSW can be largely explained in simple terms of the amplitude and phase changes of the *E* region SW2 tide in zonal wind.

Appendix: Ionospheric Dynamo Theory in a Simplified Configuration

According to the conventional description of the ionospheric neutral-wind dynamo [e.g., *Rishbeth and Garriott*, 1969, p. 234], the neutral winds in the dynamo region set ions, but not electrons, into motion through collisions, creating an electric current. The current produced *by the neutral wind alone* needs not be divergence free. At any point where this electric current is not divergence free, electric charge accumulates so that an *electrostatic polarization field* $\mathbf{E}_p = -\nabla\Phi$ is set up, where Φ is *electric potential*. The electric potential is assumed to be constant along the geomagnetic field line. This is a highly accurate approximation or a well-understood *property* of a quasi-steady configuration [*Vasyliūnas*, 2012, p. 359]. Thus, through the *equal-potential mapping* along geomagnetic field line, the electrostatic polarization field extends from the *E* region to the *F* region of the ionosphere.

In order to see more clearly how a phase change in SW2 wind can drive a phase shift in plasma drift, we describe the basic dynamo theory in a simplified configuration. Assuming a steady state, the momentum equation describes a force balance between the *Lorentz force* and the *collisional force* [*Rishbeth and Garriott*, 1969, p. 234]

$$q\mathbf{v}\times\mathbf{B} = m\nu(\mathbf{v}-\mathbf{u}) \tag{A1}$$

where $\mathbf{v}$ is the velocity of plasma (ions or electrons) and $\mathbf{u}$ is the velocity of neutral wind, $\mathbf{B}$ is the geomagnetic field, m is the mass of plasma, ν is the collision frequency, q is the particle charge ($+e$ for ions and $-e$ for electrons). In horizontal components equation (A1) can be written in the following form

$$+qv_\phi B\cos D\sin I = m\nu(v_\theta - u_\theta) \tag{A2}$$

$$-qv_\theta B\cos D\sin I = m\nu(v_\phi - u_\phi) \tag{A3}$$

where D is the magnetic declination angle, very small in the equatorial region such that $\cos D \sim 1$; I is the magnetic dip angle, defined to be positive in the (geomagnetic) Northern Hemisphere (to the north of the magnetic equator) and negative in the (geomagnetic) Southern Hemisphere (to the south of the magnetic equator); u_θ and v_θ is the meridional component velocity, u_ϕ and v_ϕ is the zonal component velocity, all

in the geographic coordinates, positive in the directions from south to north and from west to east. From equations (A2) and (A3), we have

$$\left[1+\left(\frac{\omega_c}{\nu}\cos D\sin I\right)^2\right]v_\phi = u_\phi - \left(\frac{\omega_c}{\nu}\cos D\sin I\right)u_\theta \tag{A4}$$

where $\omega_c = qB/m$ is the (ion) cyclotron frequency (or gyrofrequency). Thus, in the Northern Hemisphere, a westward $u_\phi < 0$ and northward $u_\theta > 0$ neutral wind drives a westward ion drift $v_\phi < 0$. Since electrons are much less affected by the neutral wind and affected in the opposite sense, an eastward *electrostatic polarization field* $\mathbf{E}_p$ is set up [*Rishbeth and Garriott*, 1969, p. 234]. This eastward electric field $\mathbf{E}_p > 0$ in the *E* region extends to the *F* region through equal-potential mapping, causing an upward/polarward plasma drift according to $\mathbf{V}_d = \mathbf{E}_p \times \mathbf{B}/B^2$ [*Rishbeth and Garriott*, 1969, p. 235]. In the geomagnetic (dipole) field, a geomagnetic field line at about ±10° off the geomagnetic equator in *E* region (115 km) will map to the geomagnetic equator at *F* region (300 km), see e.g., *Rishbeth and Garriott* [1969, Figure 49 (p. 185)].

It should be noted that below about 140 km in the ionospheric *E* region $\omega_c/\nu < 1$ for ions [*Rishbeth and Garriott*, 1969, p. 246] such that $|\frac{\omega_c}{\nu}\cos D\sin I| < 1$. Hence, the meridional wind plays only a secondary role in setting up east-west electric field. This is consistent with the numerical simulation result [*Millward et al.*, 2001, Figure 9].

So, in essence, westward neutral zonal winds drag ions westward but leave electrons behind, forming an eastward polarization electric field, which produces an upward vertical plasma drift.

Acknowledgments

We thank the reviewers for their comments and suggestions which helped us clarify and extend our analyses and discussions. Funding for this work was provided by NASA Heliophysics Theory Program, NASA LWS Strategic Capabilities, and NOAA/SWPC IT support. Computational resources were provided by NOAA NCEP R&D high performance computing system and NCEP Central Computing System (CCS).

Robert Lysak thanks C.H. Lin and an anonymous reviewer for their assistance in evaluating this paper.

References

Akmaev, R. A. (2011), Whole atmosphere modeling: Connecting terrestrial and space weather, *Rev. Geophys.*, *49*(4), RG4004, doi:10.1029/2011RG000364.

Akmaev, R. A., T. J. Fuller-Rowell, F. Wu, J. M. Forbes, X. Zhang, A. F. Anghel, M. D. Iredell, S. Moorthi, and H.-M. Juang (2008), Tidal variability in the lower thermosphere: Comparison of Whole Atmosphere Model (WAM) simulations with observations from TIMED, *Geophys. Res. Lett.*, *35*, L03810, doi:10.1029/2007GL032584.

Aso, T. (1993), Time-dependent numerical modelling of tides in the middle atmosphere, *J. Geomagn. Geoelec.*, *45*, 41–63.

Aso, T., S. Ito, and S. Kato (1987), Background wind effect on the diurnal tide in the middle atmosphere, *J. Geomagn. Geoelec.*, *39*, 297–305.

Chau, J. L., N. A. Aponte, E. Cabassa, M. P. Sulzer, L. P. Goncharenko, and S. A. González (2010), Quiet time ionospheric variability over Arecibo during sudden stratospheric warming events, *J. Geophys. Res.*, *115*, A00G06, doi:10.1029/2010JA015378.

Chau, J. L., L. P. Goncharenko, B. G. Fejer, and H.-L. Liu (2011), Equatorial and low latitude ionospheric effects during sudden stratospheric warming events, *Space Sci. Rev.*, *168*(1-4), 385–417, doi:10.1007/s11214-011-9797-5.

Fang, T.-W., H. Kil, G. Millward, A. D. Richmond, J.-Y. Liu, and S.-J. Oh (2009), Causal link of the wave-4 structures in plasma density and vertical plasma drift in the low-latitude ionosphere, *J. Geophys. Res.*, *114*, A10315, doi:10.1029/2009JA014460.

Fang, T.-W., R. Akmaev, T. Fuller-Rowell, F. Wu, N. Maruyama, and G. Millward (2013), Longitudinal and day-to-day variability in the ionosphere from lower atmosphere tidal forcing, *Geophys. Res. Lett.*, *40*, 2523–2528, doi:10.1002/grl.50550.

Fuller-Rowell, T., H. Wang, R. Akmaev, F. Wu, T.-W. Fang, M. Iredell, and A. Richmond (2011), Forecasting the dynamic and electrodynamic response to the January 2009 sudden stratospheric warming, *Geophys. Res. Lett.*, *38*, L13102, doi:10.1029/2011GL047732.

Goncharenko, L. P., J. L. Chau, H.-L. Liu, and A. J. Coster (2010a), Unexpected connections between the stratosphere and ionosphere, *Geophys. Res. Lett.*, *37*, L10101, doi:10.1029/2010GL043125.

Goncharenko, L. P., A. J. Coster, J. L. Chau, and C. E. Valladares (2010b), Impact of sudden stratospheric warmings on equatorial ionization anomaly, *J. Geophys. Res.*, *115*, A00G07, doi:10.1029/2010JA015400.

Goncharenko, L. P., A. J. Coster, R. A. Plumb, and D. I. V. Domeisen (2012), The potential role of stratospheric ozone in the stratosphere-ionosphere coupling during stratospheric warmings, *Geophys. Res. Lett.*, *39*, L08101, doi:10.1029/2012GL051261.

Jin, H., Y. Miyoshi, D. Pancheva, P. Mukhtarov, H. Fujiwara, and H. Shinagawa (2012), Response of migrating tides to the stratospheric sudden warming in 2009 and their effects on the ionosphere studied by a whole atmosphere-ionosphere model GAIA with COSMIC and TIMED/SABER observations, *J. Geophys. Res.*, *117*, A10323, doi:10.1029/2012JA017650.

Liu, H., M. Yamamoto, S. Tulasi Ram, T. Tsugawa, Y. Otsuka, C. Stolle, E. Doornbos, K. Yumoto, and T. Nagatsuma (2011), Equatorial electrodynamics and neutral background in the Asian sector during the 2009 stratospheric sudden warming, *J. Geophys. Res.*, *116*, A08308, doi:10.1029/2011JA016607.

Millward, G., I. C. F. Müller-Wodarg, A. D. Aylward, T. J. Fuller-Rowell, A. Richmond, and R. J. Moffett (2001), An investigation into the influence of tidal forcing on F region equatorial vertical ion drift using a global ionosphere-thermosphere model with coupled electrodynamics, *J. Geophys. Res.*, *106*, 733–744.

Pedatella, N. M., J. M. Forbes, A. Maute, A. D. Richmond, T.-W. Fang, K. M. Larson, and G. Millward (2011), Longitudinal variations in the F region ionosphere and the topside ionosphere-plasmasphere: Observations and model simulations, *J. Geophys. Res.*, *116*, A12309, doi:10.1029/2011JA016600.

Pedatella, N. M., H.-L. Liu, A. D. Richmond, A. Maute, and T.-W. Fang (2012), Simulations of solar and lunar tidal variability in the mesosphere and lower thermosphere during sudden stratosphere warmings and their influence on the low-latitude ionosphere, *J. Geophys. Res.*, *117*, A08326, doi:10.1029/2012JA017858.

Richmond, A. D. (1995a), Ionospheric electrodynamics using magnetic apex coordinates, *J. Geomagn. Geoelec.*, *47*(2), 191–212, doi:10.5636/jgg.47.191.

Richmond, A. D. (1995b), Ionospheric electrodynamics, in *Handbook of Atmospheric Electrodynamics*, vol. 2, edited by H. Volland, pp. 249–290, CRC Press, Boca Raton, Fla.

Richmond, A. D., E. C. Ridley, and R. G. Roble (1992), A thermosphere/ionosphere general circulation model with coupled electrodynamics, *Geophys. Res. Lett.*, *19*(6), 601–604, doi:10.1029/92GL00401.

Rishbeth, H., and O. K. Garriott (1969), *Introduction to Ionospheric Physics*, 334 pp., Academic Press, New York.

Scherliess, L., and B. Fejer (1999), Radar and satellite global equatorial F region vertical model, *J. Geophys. Res.*, *104*(A4), 6829–6842, doi:10.1029/1999JA900025.

Vasyliūnas, V. M. (2012), The physical basis of ionospheric electrodynamics, *Ann. Geophys.*, *30*(2), 357–369, doi:10.5194/angeo-30-357-2012.

Wang, H., T. J. Fuller-Rowell, R. A. Akmaev, M. Hu, D. T. Kleist, and M. D. Iredell (2011), First simulations with a whole atmosphere data assimilation and forecast system: The January 2009 major sudden stratospheric warming, *J. Geophys. Res.*, *116*, A12321, doi:10.1029/2011JA017081.

Wheeler, M., and G. N. Kiladis (1999), Convectively coupled equatorial waves: Analysis of clouds and temperature in the wavenumber-frequency domain, *J. Atmos. Sci.*, *56*(3), 374–399.